Clinical Cancer Research

# Vimentin Is Required for Lung Adenocarcinoma Metastasis via Heterotypic Tumor Cell–Cancer-Associated Fibroblast Interactions during Collective Invasion

Alessandra M. Richardson[1,2,3], Lauren S. Havel[2,3], Allyson E. Koyen[1,3,4], Jessica M. Konen[1,2,3], John Shupe[2,3], W.G. Wiles IV[3,5], W. David Martin[3,5], Hans E. Grossniklaus[3,6], Gabriel Sica[3,7], Melissa Gilbert-Ross[2,3,5], and Adam I. Marcus[2,3]

## Abstract

**Purpose:** Vimentin is an epithelial-to-mesenchymal transition (EMT) biomarker and intermediate filament protein that functions during cell migration to maintain structure and motility. Despite the abundance of clinical data linking vimentin to poor patient outcome, it is unclear if vimentin is required for metastasis or is a correlative biomarker. We developed a novel genetically engineered mouse model (GEMM) to probe vimentin in lung adenocarcinoma metastasis.

**Experimental Design:** We used the *LSL-Kras*$^{G12D}$/*Lkb1*$^{fl/fl}$/*Vim*$^{-/-}$ model (*KLV*$^{-/-}$), which incorporates a whole-body knockout of vimentin and is derived from the Cre-dependent *LSL-Kras*$^{G12D}$/*Lkb1*$^{fl/fl}$ model (*KLV*$^{+/+}$). We compared the metastatic phenotypes of the GEMMs and analyzed primary tumors from the *KLV* models and lung adenocarcinoma patients to assess vimentin expression and function.

**Results:** Characterization of *KLV*$^{+/+}$ and *KLV*$^{-/-}$ mice shows that although vimentin is not required for primary lung tumor growth, vimentin is required for metastasis, and vimentin loss generates lower grade primary tumors. Interestingly, in the *KLV*$^{+/+}$ mice, vimentin was not expressed in tumor cells but in cancer-associated fibroblasts (CAFs) surrounding collective invasion packs (CIPs) of epithelial tumor cells, with significantly less CIPs in *KLV*$^{-/-}$ mice. CIPs correlate with tumor grade and are vimentin-negative and E-cadherin–positive, indicating a lack of cancer cell EMT. A similar heterotypic staining pattern was observed in human lung adenocarcinoma samples. *In vitro* studies show that vimentin is required for CAF motility to lead tumor cell invasion, supporting a vimentin-dependent model of collective invasion.

**Conclusions:** These data show that vimentin is required for lung adenocarcinoma metastasis by maintaining heterotypic tumor cell–CAF interactions during collective invasion. *Clin Cancer Res; 24(2); 420–32. ©2017 AACR.*



## Introduction

Epithelial-to-mesenchymal transition (EMT) has served as a guiding principle underlying the initiation and progression of metastatic disease (1). During EMT, epithelial cells from the primary site undergo genetic (2) and epigenetic (3) alterations that trigger cancer cell invasion. A hallmark of EMT is the loss of epithelial proteins, such as E-cadherin (4), and gain of mesenchymal proteins, such as vimentin (5). These events can be transient as cells transition through partial and reversible EMT states (6–9), and it is debated whether a full EMT is necessary for metastasis (10, 11).

Over half of all lung adenocarcinoma cases present with advanced metastatic disease, which is associated with a 5-year survival rate of 4% (12). As the driving genomic aberrations of lung adenocarcinoma have become clearer, comutations in *KRAS* and *LKB1* are recognized as major drivers of the disease (13, 14). The *KRAS*/*LKB1* comutation has previously been modeled in a Cre-dependent LSL-*Kras*$^{G12D}$, *Lkb1*$^{fl/fl}$ genetically engineered mouse model (GEMM; ref. 15) to investigate this comutation in the context of metabolism (16), therapeutic response (17, 18), and microenvironment remodeling (19). In this GEMM, primary lung tumors develop at 8 to 10 weeks with 52% of mice having metastatic disease to draining lymph nodes (15, 18). When Cre is delivered intranasally via lentiviral infection, 100% of primary tumors are lung adenocarcinomas that reproduce the stages of tumor progression from adenocarcinoma *in situ* to invasive disease (18).

To assess EMT in lung adenocarcinoma, and more specifically the role of the canonical mesenchymal marker vimentin, we generated an *LSL-Kras*$^{G12D}$/*Lkb1*$^{fl/fl}$/Vim$^{-/-}$ (*KLV*$^{-/-}$) metastatic lung adenocarcinoma GEMM model, which contains a

[1]Cancer Biology Graduate Program, Emory University, Atlanta, Georgia. [2]Department of Hematology and Medical Oncology, Emory University, Atlanta, Georgia. [3]Winship Cancer Institute of Emory University, Atlanta, Georgia. [4]Department of Radiation Oncology, Emory University, Atlanta, Georgia. [5]The Cancer Animal Models Shared Resource. [6]Department of Ophthalmology, Emory University, Atlanta, Georgia. [7]Department of Pathology and Laboratory Medicine, Emory University, Atlanta, Georgia.

**Note:** Supplementary data for this article are available at Clinical Cancer Research Online (http://clincancerres.aacrjournals.org/).

**Corresponding Authors:** A.I. Marcus, The Cancer Animal Models Shared Resource, Winship Cancer Institute, Atlanta, GA, 30322. Phone: 404-778-4597; Fax: 404-778-5530; E-mail: aimarcu@emory.edu; and M. Gilbert-Ross, Phone: 404-712-8370; E-mail: mmgilbe@emory.edu

**doi:** 10.1158/1078-0432.CCR-17-1776

## Translational Relevance

Clinical data have historically linked vimentin expression to poor patient prognosis; however, it is unclear if vimentin is required for metastasis; therefore, a genetically engineered mouse model LSL-*Kras*$^{G12D}$/*Lkb1*$^{fl/fl}$/*Vim*$^{-/-}$ model (*KLV*$^{-/-}$) was developed that is a whole-body vimentin knockout crossed with the conditional Cre-dependent metastatic lung adenocarcinoma model. In this model, vimentin is not required for primary tumor growth, but is required for tumor invasion and metastasis. In *KLV*$^{+/+}$ mice, vimentin is not expressed in tumor cells but in collagen-secreting cancer-associated fibroblasts (CAFs) surrounding heterotypic collective tumor invasion packs (CIPs) adjacent to the primary tumor and in metastatic lymph nodes. Tumor cell CIPs are vimentin-negative and E-cadherin–positive, indicating a lack of cancer epithelial-to-mesenchymal transition. A similar pattern is observed in human lung adenocarcinoma samples during early-stage dissemination. Taken together, vimentin is necessary for early-stage lung adenocarcinoma dissemination by functioning in heterotypic tumor cell–CAF interactions during lung cancer invasion, suggesting that vimentin can serve as a target for preventing lung metastasis.

whole-body vimentin knockout (20). Vimentin is an intermediate filament protein, which is associated with increased metastatic potential (21), high nuclear grade (22), and poor overall survival (23) across most solid tumor types including lung, prostate, and breast cancers (24–26). Because vimentin is integral for the structural integrity of the cell (27), lamellipodia formation (28), and adhesion signaling (29, 30), downregulating vimentin expression is sufficient to alter cell morphology *in vitro* (31) as well as inhibit cell motility and invasion (32).

The data presented here from GEMMs, human lung adenocarcinoma samples, and *in vitro* 3D models show that vimentin is required for lung adenocarcinoma to metastasize at an early stage by acting in cancer-associated fibroblasts (CAF) that surround epithelial-like collective invasion packs (CIPs). These data support the concept that vimentin is critical for lung adenocarcinoma metastasis and could be a potential target for antimetastatic therapies.

## Materials and Methods

### Transgenic mouse model

*KLV*$^{-/-}$ mouse was generated by crossing the LSL-Kras$^{G12D}$/LKB1$^{fl/fl}$ mouse (15) with the Vimentin$^{-/-}$ (20) mouse until a homozygous *KLV*$^{-/-}$ mouse was generated. *KLV*$^{-/-}$ mouse took approximately four generations over 7 months to create. *KLV*$^{+/-}$ mice were generated by crossing *KLV*$^{+/+}$ mice with *KLV*$^{-/-}$ mice. All mice were housed and treated according to Institutional Animal Care and Use Committee protocol #2003525 by the Emory University Division of Animal Resources. *Kras*- and *Lkb1*-mutant mice were purchased from The Jackson Laboratory. Vimentin-null mice were obtained from the EMMA repository (20). Lentiviral Cre ($1.2 \times 10^7$ i.u.) was administered intranasally to mice 8 to 12 weeks old that were sedated with Avertin (20 mg/mL working dilution). Infected mice were then monitored until tumorigenic symptoms (i.e., weight loss greater than 10%, respiratory distress, inactivity) presented. All mice infected with lentiviral Cre were monitored to a 25-week postinfection endpoint and were sacrificed prior if they presented with clinical symptoms including weight loss, respiratory distress, and/or hunching. Upon sacrifice, lungs and mediastinal lymph nodes were harvested in either 10% formalin or flash frozen in *OCT* pending use.

### Human lung adenocarcinoma tissue

Deidentified human lung adenocarcinoma tissue is a mixed cohort of samples from Emory and Wellstar tumor banks and Emory clinical formalin-fixed paraffin-embedded (FFPE) tumor specimens (IRB00009857). All Emory samples were sequenced using a workflow described (18). Lung adenocarcinoma staging was performed by a board-certified thoracic pathologist according to the AJCC Cancer Staging Manual 7$^{th}$ Edition. Vimentin immunohistochemistry (IHC) was scored by a board-certified thoracic pathologist with a 40X objective on a scale from 0 to 3 based on stain intensity and was stratified by stromal or tumor compartment. *Q* score was determined by the multiplication of stain intensity by percentage of cells staining at that intensity for a given cell compartment (i.e., 30% of stromal cells at level 3 stain has *Q* score of 90).

### Immunohistochemistry

FFPE tissues were hydrated in a series of washes from xylenes to ethanol dilutions to water. Heat-mediated antigen retrieval was conducted with citrate buffer when necessary. Endogenous peroxidase activity was blocked with 3% hydrogen peroxide. Samples were blocked with 2.5% normal goat serum (Vector Labs) and incubated in primary antibody overnight in 1:1 NGS:PBS solution (Vimentin R28 Cell Signaling Technology 1:300, alpha SMA Invitrogen 1:1,000, Pro-SPC Santa Cruz FL-197 1:150, CD31 ab28364 1:50 CD3 ab16669 1:100). Samples were incubated in secondary antibody (Rabbit 1:200), biotin, and streptavidin (Vector Labs) according to kit protocol. Staining was developed using Peroxidase Substrate Kit DAB (Vector Labs). Proliferation was measured by staining for Ki67 (ab16667, 1:200) using IMMpact Kit (Vector Labs).

### Immunofluorescence

***Tissue.*** Tissue sections frozen in OCT Compound were sliced in 10 μm sections and fixed in 100% acetone. Sections were stored at −80°C until used. Sections were blocked for 1 hour in 10% normal goat serum in PBS. Primary antibodies were incubated in PBS overnight for the following antibodies at indicated concentrations: vimentin R28 Cell Signaling Technology 1:50, F4/80 Abcam 1:100, FSP1 ab27957 1:200. FFPE tissues were hydrated as described above. Heat-mediated antigen retrieval was also conducted as above. A blocking buffer of 5% BSA in PBS was used. Primary antibodies were incubated at 4°C overnight in 1% BSA in PBS (FSP1 ab27957 1:200; E-cadherin BD Biosciences 610181 1:1,000). Secondary antibodies were incubated on tissues for 1 hour (1:1,000).

***Cells.*** CAFs were fixed and stained as described (30). Primary antibodies were diluted in 5% normal goat serum (Vimentin R28 Cell Signaling Technology 1:50) and added to cells on coverslips overnight at 4°C. The coverslips were mounted on glass slides

using Prolong diamond mounting medium (Invitrogen). The slides were imaged using Leica SP8 confocal microscope.

***Spheroids.*** Spheroids embedded in matrigel were fixed with 4% paraformaldehyde for 20 minutes. Glycine rinse (TBS/glycine 130 mmol/L NaCl, 7 mmol/L $Na_2HPO_4$, 3.5 mmol/L NaH2PO4, 100 mmol/L glycine) performed three times for 10 minutes at room temperature. The immunofluorescence (IF) buffer used for protocol consisted of 130 mmol/L NaCl, 7 mmol/L $Na_2HPO_4$, 3.5 mmol/L $NaH_2PO_4$, 0.5% Triton X-100, and 0.5%, Tween-20. Samples were blocked in IF buffer supplemented with 3% BSA, 5% goat serum, and 0.3% Triton X-100 for 2 hours at room temperature. Primary antibodies incubated overnight in blocking buffer (FSP1 1:250) at room temperature. IF buffer was used for three 20-minute washes. Secondary antibody was diluted 1:500 in blocking buffer (Phalloidin 488 1:40 and DAPI added) and incubated at room temperature overnight. Fluorescence was imaged on Confocal Leica SP8 microscope.

### Multiphoton microscopy

Second harmonic generation (SHG) images of hematoxylin and eosin (H&E) sections were taken using a Zeiss Axio Examiner Z1 microscope with 20X water immersion objective (1.0 NA DIC [UV] VIS-IR) as described (33). The SHG signal was obtained using a band pass cube of 380 to 430 nm. Images were taken with a Coherent Chameleon Verdi laser at 820 nm wavelength. Z-stack images were taken with a 1-μm interval.

### Western blot

Lung tissue was harvested and flash frozen in liquid nitrogen. Frozen tissue was cut into 2-mm pieces and ground in glass mortar and pestle in 1 mL of lysis buffer TNES buffer (50 mmol/L Tris, pH 7.5, 100 mmol/L NaCl, 2 mmol/L EDTA, 1% Nonidet P-40, 1X Roche Complete Protease Inhibitors, 10 mmol/L NaF, 1 mmol/L NaVO4, 2 mmol/L sodium pyrophosphate, and 2 mmol/L β-glycerophosphate). Mixture was further homogenized with a sonicator. Lysate was centrifuged, and supernatant was collected. Protein assay and Western blot were performed as described (30). Primary antibody, diluted in either 5% BSA in TBST (Vimentin R28 Cell Signaling Technology 1:1,000) or 5% milk in TBST (Tubulin Millipore MAB1864 1:20,000, GAPDH CST 1:30,000), was added to membrane overnight. Secondary antibodies were incubated at a concentration of 1:1,000 in 5% milk in TBST for 1 hour.

### Cell culture

H460 lung cancer cell line was purchased from the ATCC and subcultured in RPMI 1640 media supplemented with 10% FBS, 1% penicillin/streptomycin, and 1% kanamycin. Human lung adenocarcinoma CAFs were purchased from Vitro Biopharma and subcultured in MSC Gro VitroPlus III, Low Serum media supplemented with 1% penicillin/streptomycin and 1% kanamycin. All cells were cultured in a humidified chamber at 37°C with 5% $CO_2$. Experiments were performed with cells below passage 10. All cells were verified as mycoplasma-free on October 4, 2017, by DAPI staining.

### Stable cell line generation

For the production of stable vimentin knockdown CAFs, pLKO.1 vector and vimentin shRNA virus described previously (30) were added to cells 1:2 in media with 8 μg/mL polybrene three times. Cells expressing the constructs were selected using puromycin 2 μg/mL treatment.

### 3D spheroid invasion assay

Spheroids of H460s, CAFs, and H460/CAF 50/50 cocultures were generated as described (18). Spheroids were collected and resuspended in 250 μL of 2.0 mg/mL MatriGel (VWR) in a 35-mm Dish with a 14-mm bottom well (Cellvis), and a coverslip was attached with Vaseline. After 45-minute incubation at 37°C, 2 mL of media was added. Images were taken at 0 and 24 hours on Olympus IX51 microscope. Spheroid invasion was quantified using ImageJ (NIH). For 3D IF, spheroids were formed as described above. Each well of a 96-well flat-bottomed plate (Corning) was coated with 8 mg/mL MatriGel. Spheroids were collected and resuspended in 50 μL of 2.0 mg/mL MatriGel. After a 45-minute incubation at 37°C, 100 μL of media was added. Spheroids were allowed to invade for 48 hours.

### PCR

Tissue was collected from candidate pups prior to weaning. Genomic DNA was extracted using Alkaline Lysis Buffer at 100°C for 45 minutes. A 40 mmol/L Tris-HCL Neutralization Buffer was then added, and samples were stored at −20°C. PCR was performed using a GoTaq Flexi system from Promega. Samples were run on Biorad iCycler at recommended annealing temperatures.

### Image analysis

H&E and IHC-stained tissue samples were imaged on the Zeiss Axioplan 2 widefield microscope, or whole slides were scanned into ImageScope software. IF images were taken on the Confocal Leica SP8. All images were analyzed with ImageJ and Photoshop Elements. CellProfiler was used for fluorescent image quantification. Imaris software was used for vim/FSP1 colocalization analysis where a mask was generated for each marker and then a colocalization mask was generated from this. The 2D histogram was generated in Imaris by removing background levels of each marker. Pearson's coefficient was generated from the histogram. Imaris was also used for CAF cell size analysis.

### Tumor histology

Stromal and tumor compartments in *KLV* mouse were identified by a board-certified thoracic pathologist. *KLV* model tumor grading was performed as described (34).

### Statistical analysis

*P* values of significance were obtained using a Fischer exact test, $\chi^2$ test, or unpaired *t* test when comparing two groups (i.e., $KLV^{+/+}$ vs. $KLV^{-/-}$ or metastatic vs. nonmetastatic). Data with more than two groups were analyzed by one-way ANOVA followed by Tukey's multiple comparisons test. Analysis of vimentin IHC in patient samples was performed using the Wilcoxon Rank Sum test. Kaplan–Meier curves were analyzed by Mantel–Cox and Gehan–Breslow–Wilcoxon tests.

## Results

### Generation of a $Kras^{G12D}/LKB1^{fl/fl}/Vim^{-/-}$ GEMM ($KLV^{-/-}$)

Metastasis is well characterized in the $LSL\text{-}Kras^{G12D}/LKB1^{fl/fl}$ ($KLV^{+/+}$) model (15, 18), where approximately 52% of mice that develop primary lung tumors at 8 to 10 weeks also develop metastasis to mediastinal lymph nodes at 12 to 16 weeks (18). A whole-body $vimentin^{-/-}$ mouse (20) was crossed to this $KLV^{+/+}$ mouse to test the hypothesis that vimentin is necessary for metastatic disease. Through this cross, a novel $LSL\text{-}Kras^{G12D}$,

*LKB1*$^{fl/fl}$,*Vim*$^{-/-}$ (*KLV*$^{-/-}$) mouse was generated (Supplementary Fig. S1A) that lacks vimentin expression throughout and has the *LSL-Kras*$^{G12D}$,*LKB1*$^{fl/fl}$ conditionally mutated in the lungs via intranasal delivery of lentiviral Cre recombinase. Disruption of the vimentin allele and lack of protein expression in the *KLV*$^{-/-}$ mouse were validated by RT-PCR, Western blotting, and IF (Supplementary Fig. S1B–S1D). Disruption of one vimentin allele in the heterozygous *KLV*$^{+/-}$ mouse did not greatly reduce vimentin protein expression (Supplementary Fig. S1C and S1D). These results demonstrate the development of a novel *KLV*$^{-/-}$ GEMM to probe the role of vimentin in lung adenocarcinoma metastasis.

### *KLV*$^{+/+}$ and *KLV*$^{-/-}$ mice have a similar primary tumor burden

*KLV*$^{+/+}$ and *KLV*$^{-/-}$ were infected intranasally with Cre lentivirus, and a comparison of tumor burden between the two genotypes (either at 25 weeks or before due to morbidity) revealed no significant differences in primary tumor initiation or growth (Table 1 and Fig. 1A). In both genotypes, 100% of primary tumors were lung adenocarcinomas with no significant difference in tumor incidence (Table 1). Both *KLV*$^{+/+}$ and *KLV*$^{-/-}$ mice generated primary lung tumors (Fig. 1A) without a significant difference in lung weight (Fig. 1B) or tumor multiplicity (number of tumor foci per H&E slice; Fig. 1C). Tumor histology was similar across genotypes with both *KLV*$^{+/+}$ and *KLV*$^{-/-}$ mice developing tumors with and without invasive fronts (Fig. 1D). Proliferative index using Ki-67 staining was also not significantly different between the two genotypes (Fig. 1E and F). Based on these data, we conclude that vimentin loss does not affect primary lung tumor initiation or growth. A Kaplan–Meier curve to clinical symptoms shows that *KLV*$^{-/-}$ mice have decreased survival compared with *KLV*$^{+/+}$ (Supplementary Fig. S2).

### Vimentin-null mice have reduced metastatic disease and less focal invasion

The *KLV*$^{+/+}$ model develops robust primary lung tumors and metastasis to the mediastinal lymph node (15, 18). We leveraged this phenotype to investigate how the vimentin loss affects the metastatic potential of *Kras/Lkb1* comutated lung adenocarcinomas. Vimentin loss in *KLV*$^{-/-}$ mice results in 54% less mediastinal lymph nodes metastasis compared with *KLV*$^{+/+}$*mice* (Fig. 2A and B). In mice with clinical symptoms (respiratory distress, weight loss, hunching), vimentin loss was associated with significantly less metastatic disease to the draining lymph nodes compared with *KLV*$^{+/+}$ mice (Fig. 2C). In addition to decreased incidence of lymph node metastasis, vimentin loss in the *KLV*$^{-/-}$ is associated with significantly less invasive foci than *KLV*$^{+/+}$ mice tumors as measured by the number of invasive fields (defined as a field with focal invasion) per mouse (Fig. 2D).

To assess the impact of vimentin loss on tumor progression, primary tumors of *KLV*$^{+/+}$ and *KLV*$^{-/-}$ were graded on a scale of 1 to 4 with grade 1 tumors classified as atypical adenomatous hyperplasia and grade 4 tumors demonstrating stromal reaction in addition to irregular mitoses and invasive borders along lymphatic vessels. Higher tumor grade is also associated with more invasive and metastatic tumors (34). Based on this analysis, the *KLV*$^{+/+}$ mice developed significantly more high-grade tumors than *KLV*$^{-/-}$ mice (Fig. 2E), further supporting the claim that vimentin loss reduces metastatic disease and tumor progression. Taken together, these data show that vimentin is required for efficient metastasis in *Kras/Lkb1* comutated lung adenocarcinoma.

**Table 1.** Infection rate and histology of lentiviral-Cre–treated mice of both *KLV*$^{+/+}$ and *KLV*$^{-/-}$ mice

| Genotype | Primary tumor rate | Adenocarcinoma histology |
|---|---|---|
| *KLV*$^{+/+}$ | 17/26 (66%) | 17/17 (100%) |
| *KLV*$^{-/-}$ | 47/70 (67%) | 47/47 (100%) |

### Vimentin is required for CIP formation

To determine vimentin localization within the primary tumor, vimentin IHC was performed on *KLV*$^{+/+}$ primary tumor samples (Fig. 3A). The vimentin antibody was validated for specificity by IHC in vimentin-null tissue and by Western blot (Supplementary Fig. S3). To our surprise, in *KLV*$^{+/+}$ samples, vimentin expression was absent in tumor cells but present in the stromal niche often surrounding tumor cells that appear to have budded off from the primary tumor. We previously termed these tumor cell histologies CIPs (18). CIPs are surrounded by vimentin-positive, elongated stromal cells that resemble fibroblasts in morphology (Fig. 3A).

CIPs are positive for the lung adenocarcinoma marker pro-SPC (ref. 35; Fig. 3B), indicating their type II pneumocyte origin, retain epithelial morphology (nonelongated), and express E-cadherin (18), while lacking vimentin protein expression (Fig. 3A). This pattern suggests that tumor cells within CIPs retain homotypic cell contacts and are likely not undergoing a traditional EMT. CIPs range in size from 5 to 25 cells (Fig. 3C) and are found within this range in *KLV*$^{+/+}$ and *KLV*$^{-/-}$ primary tumor samples. CIP density in each genotype was assessed, and these data show that *KLV*$^{-/-}$ mice have significantly less CIPs per invasive field than *KLV*$^{+/+}$ mice overall (Fig. 3D). When CIP density is stratified by tumor grade (Fig. 3E), high-grade *KLV*$^{-/-}$ tumors have significantly less CIPs than high-grade *KLV*$^{+/+}$ tumors, indicating that vimentin is required to maintain CIP density in invading tumors. Further, these data indicate that within the *KLV* models, the predominant role of vimentin lies within stromal cells rather than tumor cells.

To determine the role of CIPs in tumor progression and metastasis, CIP density and invasive area were stratified by extent of disease or tumor stage. These data demonstrate that CIPs are found in both early (nonmetastatic) and late (metastatic) stage *KLV* tumors (Fig. 3F and G) with significantly higher CIP density and invasion in late-stage tumors. To probe CIP biology, IF of extracellular matrix (ECM) components was performed. Fibronectin staining reveals that cancer cells themselves are negative for fibronectin, but fibronectin is expressed in the regions surrounding emerging CIPs at the invasive front of the primary tumor in both *KLV*$^{+/+}$ and *KLV*$^{-/-}$ samples (Fig. 3H; Supplementary Fig. S4A). Interestingly, fibronectin expression is lost in CIPs farther away from the primary tumor, suggesting that fibronectin may only be important for early invasion events (Fig. 3H).

Second harmonic generation imaging was performed to assess the collagen ECM which showed high levels of aligned collagen at the invasive front of the primary tumor and surrounding CIPs in the *KLV* models (Fig. 3I; Supplementary Fig. S4B). This aligned collagen persisted at metastatic lymph nodes, indicating that collagen alignment and secretion are maintained at the distant metastatic site (Fig. 3I). To probe cancer invasion and EMT, IF of TGFβ1 ligand was performed in primary tumor samples (Supplementary Fig. S4C). High expression was observed in areas of focal invasion at or near the primary tumor indicating TGFβ1 is promoting cancer invasion and progression in the *KLV* models without inducing some canonical EMT markers.

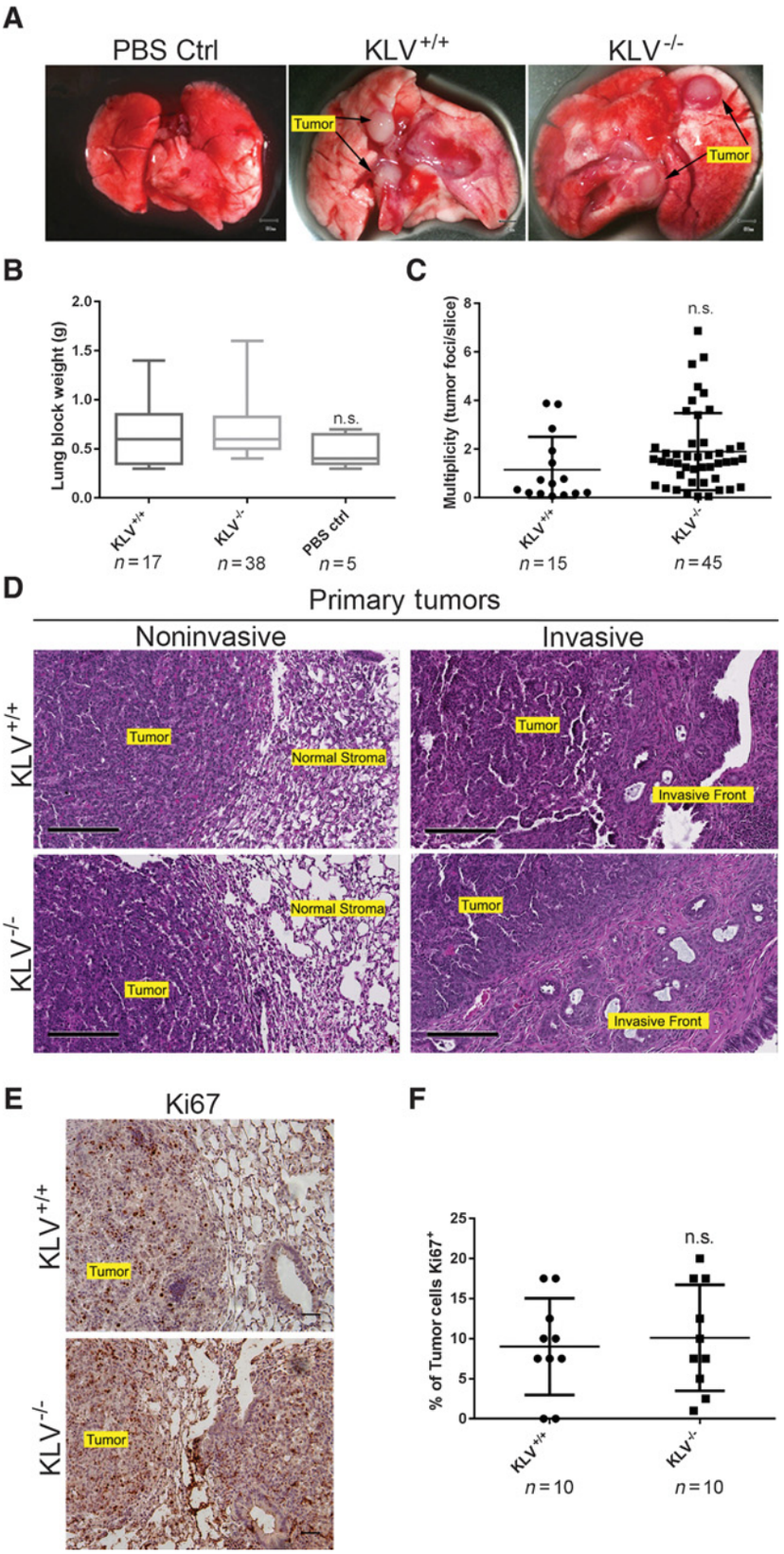


**Figure 1.**

*KLV*$^{+/+}$ and *KLV*$^{-/-}$ mice have a similar primary tumor burden. **A,** Representative images of PBS control, *KLV*$^{+/+}$, and *KLV*$^{-/-}$ lungs (scale = 50 mm). **B,** Graphs showing weight of PBS control, *KLV*$^{+/+}$, and *KLV*$^{-/-}$ lungs. Statistical significance was determined by one-way ANOVA and Tukey's multiple comparisons test ($P < 0.05$). **C,** Tumor multiplicity of *KLV*$^{+/+}$ and *KLV*$^{-/-}$ mice quantified as the number of tumor foci per H&E lung slice. Statistical significance was determined by the unpaired *t* test ($P < 0.05$). **D,** Representative H&E sections of *KLV*$^{+/+}$ and *KLV*$^{-/-}$ primary tumors (scale = 200 μm). **E,** IHC of Ki67 in *KLV*$^{+/+}$ and KLV$^{-/-}$ primary tumors. **F,** Quantification of percentage of Ki67-positive tumor cells. Statistical significance was determined by the unpaired *t* test $P > 0.05$.

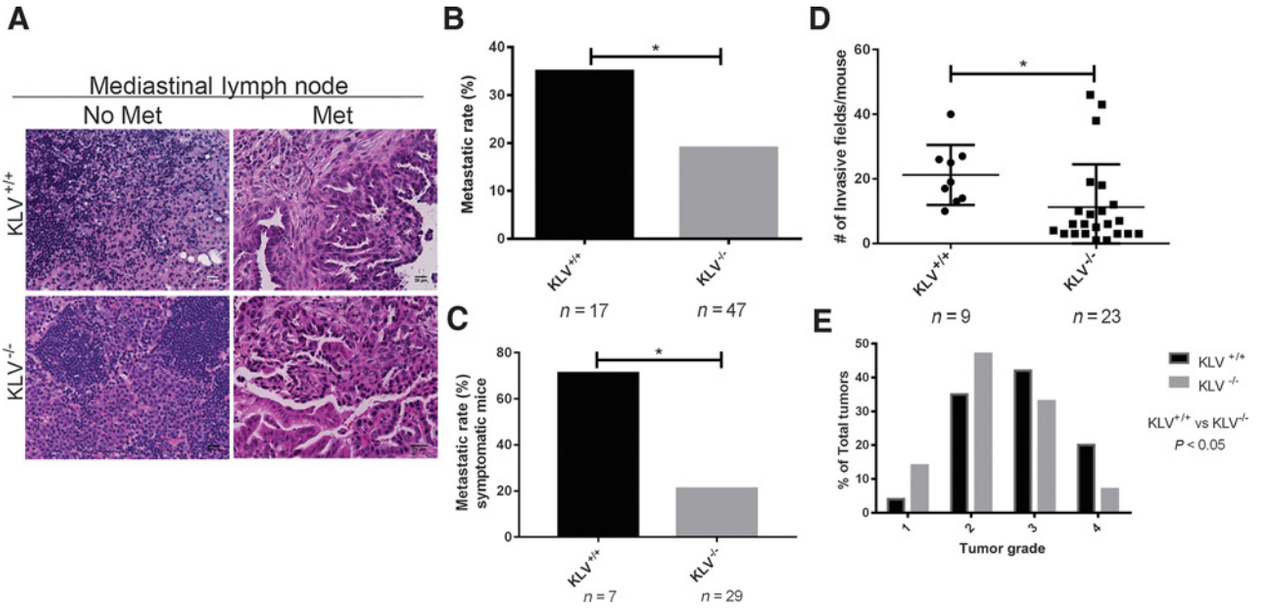


**Figure 2.**

Vimentin depletion inhibits invasion and metastasis. **A,** Representative H&E images of lung draining lymph nodes of LV-Cre–infected mice (scale = 20 μm). **B,** Metastatic incidence by *KLV* genotype. Statistical significance was determined by the Fisher exact test ($P < 0.05$). **C,** Metastatic incidence of mice sacrificed prior to 25-week endpoint due to lung cancer symptoms. Statistical significance was determined by the Fisher exact test ($P < 0.05$). **D,** Quantification of invasive fields per mouse by genotype. Statistical significance was determined by the unpaired *t* test ($P < 0.05$). **E,** *KLV* tumor grading by genotype. Statistical significance was determined by the $\chi^2$ test ($P < 0.05$).

### Vimentin$^+$ CAFs surround CIPs

To characterize vimentin-positive cells surrounding CIPs, FSP1 (Fibroblast Specific Protein 1) and alpha-Smooth Muscle Actin (α-SMA) were used to mark CAFs (36). Dual labeling of vimentin and FSP1 in $KLV^{+/+}$ primary tumor samples demonstrates that vim$^+$ stromal cells are also FSP1$^+$ (Fig. 4A). FSP1$^+$/vim$^+$ cells are randomly localized within the primary tumor (Fig. 4A, left) but surround CIPs at sites of focal invasion (Fig. 4A, right). Quantitative analysis of FSP1$^+$/vim$^+$ cells surrounding CIPs shows colocalization between vimentin and FSP1 (Pearson coefficient = 0.59; Fig. 4B). IHC of serial sections shows that vim$^+$ cells are also α-SMA$^+$ (Supplementary Fig. S5A). These data strongly suggest that vim$^+$ cells are CAFs. FSP1$^+$ CAFs are found at the invasive fronts of both $KLV^{+/+}$ and $KLV^{-/-}$ primary tumors (Supplementary Fig. S5B); however, the significantly greater extent of focal invasion in $KLV^{+/+}$ tumors (Fig. 3D) indicates increased CAF recruitment in this model.

Because many tumor-promoting components of the tumor microenvironment express vimentin, several members of the microenvironment were probed within the *KLV* models, including macrophages, inflammatory cells, and vascular cells. IF of tumor-associated macrophages with F4/80 in $KLV^{+/+}$ and $KLV^{-/-}$ primary tumor samples shows no significant difference in macrophage recruitment (Supplementary Fig. S6). IHC of a Pan T-cell marker (CD3) and endothelial marker (CD31) also demonstrated no difference in recruitment of these factors (Supplementary Fig. S7A and S7B). Taken together, these data indicate that vimentin loss does not impede the recruitment of vascular or inflammatory cells to the primary tumor microenvironment.

To determine the relationship between CAF recruitment and metastatic disease, the presence or absence of CAFs was stratified by genotype and metastatic phenotype. These results show that 100% of metastatic mice contained CAFs at the primary tumor site (Fig. 4C), but less than 50% of nonmetastatic mice had CAFs recruited to the primary tumor in both $KLV^{+/+}$ and $KLV^{-/-}$ genotypes. Vimentin IHC identified that CAFs are also found surrounding CIPs at the metastatic lymph nodes, demonstrating that CAFs are important components of the tumor microenvironment at the secondary site (Fig. 4D) and perhaps travel with tumor cells to the lymph node. These data suggest that CAF recruitment contributes to tumor metastasis by promoting CIP formation and facilitating metastasis to the secondary site.

### Vimentin regulates CAF invasion and stroma–cancer cell cross-talk

To probe the mechanisms of the heterotypic tumor cell–CAF interactions and CAF recruitment found in the *KLV* models, *in vitro* studies were performed. Stable knockdown of vimentin was achieved in human lung adenocarcinoma CAFs via shRNA (Fig. 5A and B). CAFs lacking vimentin (shVIM19 and shVIM22) were significantly smaller than pLKO.1 vector control (Fig. 5C and D). To test the hypothesis that vimentin depletion inhibits CAF invasion in the *KLV* models, 3D spheroid invasion assays were performed with pLKO.1 and shVIM CAFs embedded in MatriGel (Fig. 5E). Results show that shVIM CAFs invaded significantly less than pLKO.1 CAFs (Fig. 5F), supporting the hypothesis that CAF motility is impaired with vimentin loss in the *KLV* models.

Coculture 3D spheroid invasion assays were then performed to assess heterotypic cancer cell–CAF interactions (Fig. 5G). Invasion analysis revealed that the addition of CAFs to spheroids of H460s

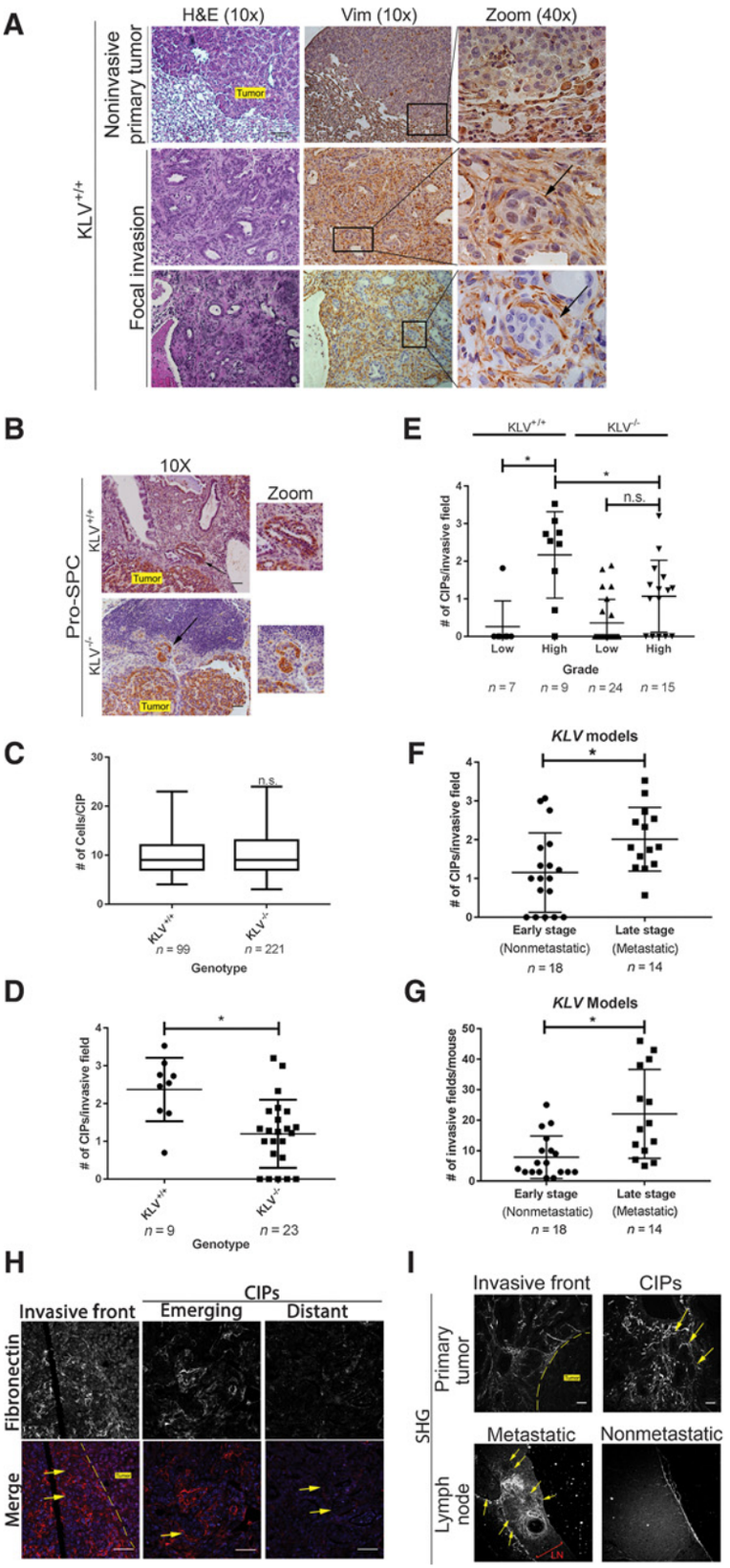


**Figure 3.**

Vimentin is required for CIP formation. **A,** Immunohistochemical staining of vimentin in $KLV^{+/+}$ mice with serial H&E sections. Black arrows mark CIPs (10x scale = 100 μm, 40x = 20 μm). **B,** Representative Pro–SPC-stained sections of $KLV^{+/+}$ and $KLV^{-/-}$ primary tumors with CIPs marked by black arrows. **C,** Quantification of number of cells per CIP in both $KLV^{+/+}$ and $KLV^{-/-}$ mice. Statistical significance determined by the unpaired *t* test ($P > 0.05$). **D,** Quantification of CIPs per invasive field in $KLV^{+/+}$ and $KLV^{-/-}$ mice. Statistical significance determined by the unpaired t test ($P < 0.05$). **E,** CIPs per invasive field stratified by genotype and tumor grade. Statistical significance determined by ANOVA and Tukey's multiple comparisons test ($P < 0.05$). **F,** Quantification of CIPs per invasive field stratified by metastatic phenotype in *KLV* models ($P < 0.05$). **G,** Quantification of invasive fields by metastatic phenotype in *KLV* models Statistical significance determined by the unpaired *t* test ($P < 0.05$). **H,** IF of fibronectin in *KLV* primary tumor samples at the invasive front, emerging from the primary tumor, and at site distant from the primary tumor. Yellow arrows mark CIPs with invasive frontmarked by dashed line (scale = 50 μm). **I,** Second harmonic generation imaging of collagen in *KLV* samples at the invasive front and surrounding CIPs in both primary tumor and metastatic lymph node. Yellow arrows mark CIPs with invasive front marked by dashed line (scale = 50 μm).

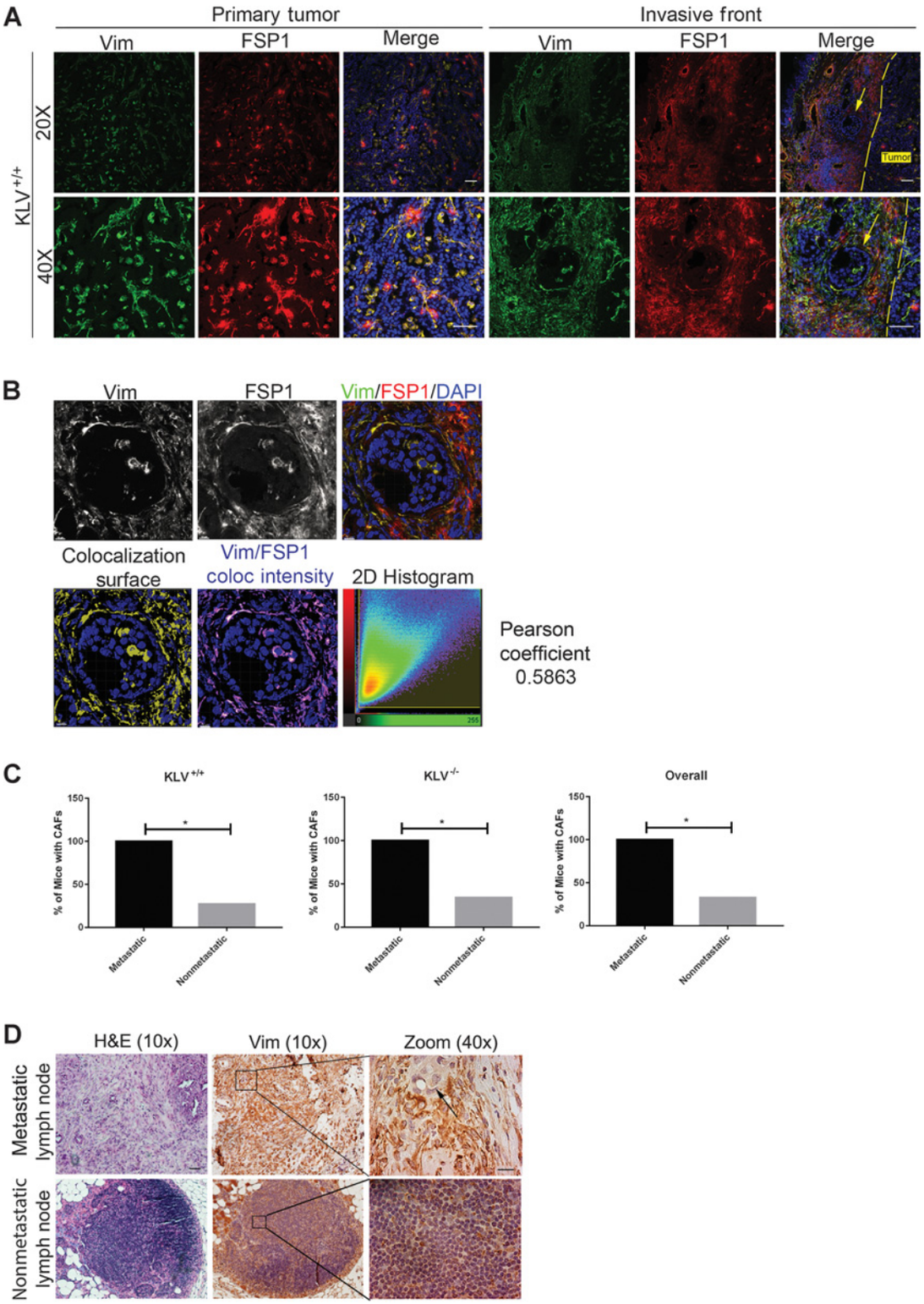


**Figure 4.**

Vimentin$^{+}$ CAFs surround CIPs. **A,** IF of vimentin (488) and FSP1 (555) on primary tumors $KLV^{+/+}$ mice (scale = 50 μm). **B,** Colocalization of vimentin and FSP1 staining (scale = 10 μm). **C,** Quantification of percentage of mice of each genotype with CAFs stratified by metastatic or nonmetastatic phenotypes. **D,** Immunohistochemical staining of vimentin in the metastatic and nonmetastatic lymph nodes (scale bars: 10x = 100 μm, 40x = 20 μm).

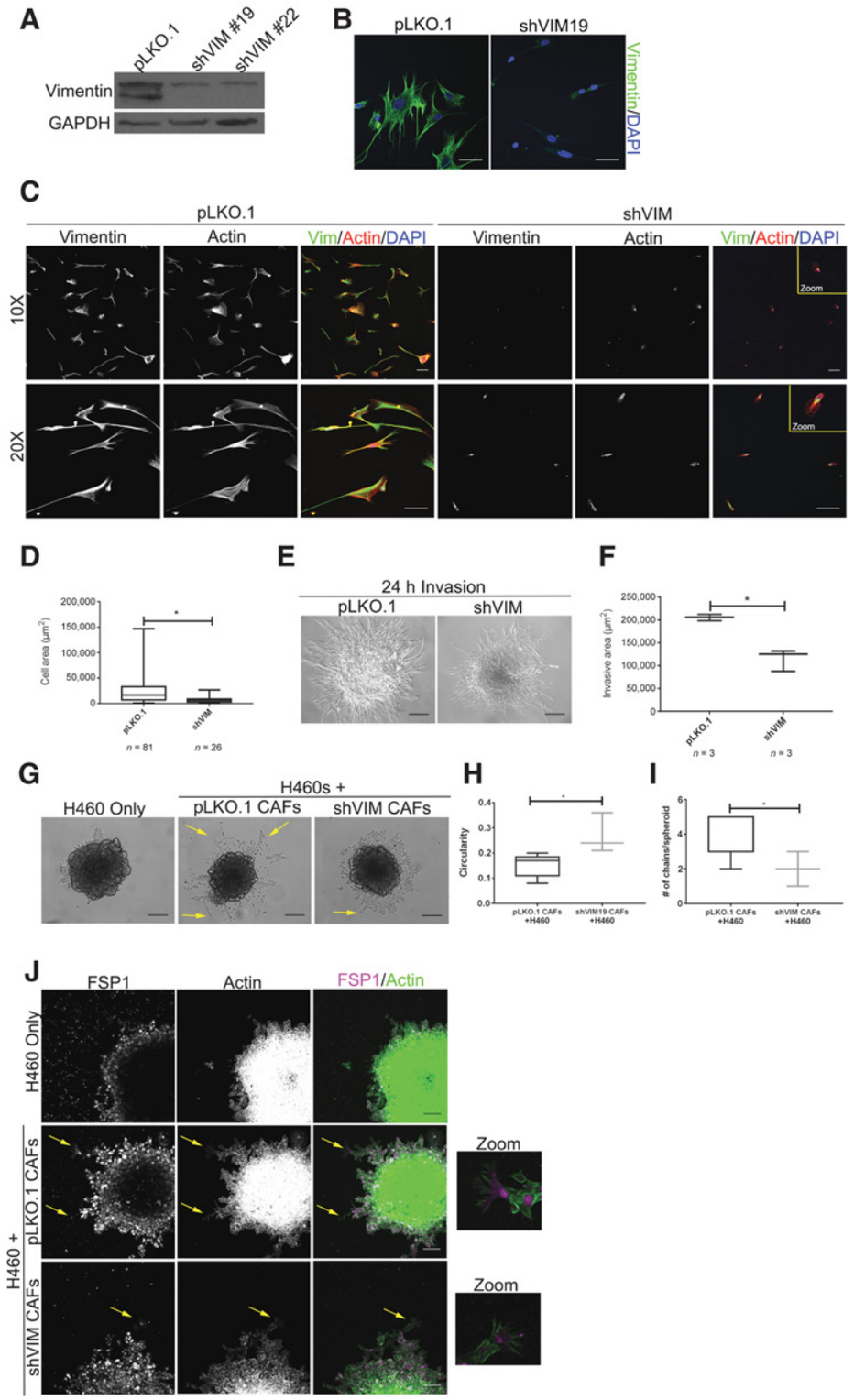


**Figure 5.**
Vimentin regulates CAF invasion and stroma-cancer cell cross-talk. **A,** Western blot demonstrating generation of shVIM CAFs with two different shRNA clones. **B,** IF of vimentin in pLKO.1 andshVIM19 CAFs (scale = 50 μm). **C,** IF of actin and vimentin in pLKO.1 and shVIM CAFs demonstrating cell size (10x scale = 100 μm, 20x scale = 100 μm). **D,** Quantification of cell area of pLKO.1 and shVIM CAFs. Significance determined by the unpaired *t* test ($P < 0.05$). **E,** Representative images of spheroid invasion assay with pLKO.1 and shVIM CAFs in matrigel (scale = 100 μm). **F,** Quantification of invasive area in spheroid invasion assay. Significance determined by the unpaired *t* test ($P < 0.05$). **G,** Representative images of coculture spheroid invasion assay with H460 lung cancer line alone or in combination with pLKO.1 or shVIMCAFs (scale = 100 μm). **H,** Circularity of invasive areas in representative trial (3 total trials) of coculture spheroids with pLKO.1 ($n = 6$) or shVIM ($n = 3$) CAFs. Value of 1 = perfect circle. Significance determined by the unpaired *t* test ($P < 0.05$). **I,** Quantification of invasive chains in representative coculture spheroids with pLKO.1 or shVIM CAFs. Significance determined by the unpaired *t* test ($P < 0.05$). **J,** Representative images of IF of FSP1 and phalloidin in coculture spheroids. Yellow arrows mark CAFs positive for cytoplasmic FSP1 leading invasive chain of H460s (scale = 100 μm).

(lung adenocarcinoma cell line) decreases circularity, a surrogate for collective invasion branching (i.e., increased circularity means less CIPs; Supplementary Fig. S8). Coculture spheroids with shVIM CAFs exhibit significantly higher circularity (decreased branching) compared with those with pLKO.1 CAFs (Fig. 5H). These same coculture spheroids show significantly less invasive chains (37) per spheroid with shVIM CAFs compared with pLKO.1 CAFs (Fig. 5I). These data suggest impairment in shVIM

CAFs to drive collective invasion. IF of FSP1 and actin in coculture spheroids (Fig. 5J) shows that CAFs facilitate collective invasion by leading chains of H460s into the surrounding ECM. CAFs lacking vimentin expression lose the ability to lead cancer cells out of the spheroid as evidenced by the decrease in invasive branches with CAFs leading the chain (Fig. 5H). Together, these data indicate that heterotypic *in vitro* 3D invasion is vimentin-dependent and consistent with the *in vivo* GEMM results.

**Vimentin is expressed in CAFs of lung cancer patient CIPs, which lack EMT in tumor cells**

To analyze the clinical relevance of the CIP phenotype found in the *KLV* models, vimentin staining in human lung adenocarcinoma patients with varying genetic subtypes was performed to assess vimentin localization, invasive histology, and EMT (Fig. 6A). A similar pattern to the $KLV^{+/+}$ mouse samples was observed in human tissues, where the vast majority of patient samples (25 of 26) expressed vimentin in the mesenchymal stroma and not within the collectively invading cancer cells (Fig. 6A). Vimentin stain intensity was scored and was significantly higher in stromal cells compared with tumor cells across the majority of samples, independent of driver mutation (Fig. 6B). Furthermore, there were no observable differences in vimentin stromal Q score (product of stain intensity and percentage of vimentin-positive cells in stromal compartment) based upon genetic subtype (Supplementary Fig. S9).

Because tumor cells lacked vimentin staining, the epithelial cell marker, E-cadherin, was used to further probe for evidence of EMT. Tumor cells within patient CIPs were E-cadherin–positive (ref. 18; Fig. 6C) and pro–SPC-positive (Fig. 6D), which is also consistent with the data in the *KLV* models. IF of FSP1 was performed to determine if patient CIPs are surrounded by CAFs similar to the *KLV* model. These data show an expression pattern consistent with the *KLV* model in which $FSP1^+$ CAFs surround CIPs of tumor cells (Fig. 6E). Taken together, these data suggest that in human lung adenocarcinoma samples tumor cells are not undergoing EMT but instead contain invasive CIPs surrounded by $vim^+/FSP^+$ CAFs, indicating that the predominant role of vimentin in lung adenocarcinoma lies within CAFs and not tumor cells.

To determine the clinical relevance of CIPs, CIP density was stratified in human lung adenocarcinoma patient samples (Fig. 6F and G). Stage 1 patients exhibit significantly higher CIP density than higher stage patients indicating an early dissemination of CIP and CAF invasion, though there are still CIPs present in late-stage patients ($P < 0.05$). Taken together, the formation of CIPs in early-stage tumors supports an early dissemination model (38) in which metastatic seeds such as CIPs disseminate early during tumor progression.

## Discussion

Vimentin expression has historically correlated with increased metastatic potential across numerous solid tumor types (24, 39); however, a functional role for vimentin in cancer progression has yet to be elucidated. Data from the $KLV^{-/-}$ GEMM show that vimentin is required for metastasis and progression but not primary tumor formation, whereby $KLV^{-/-}$ mice had less mediastinal lymph nodes metastasis, less invasive foci, and lower grade tumors compared with their $KLV^{+/+}$ counterparts (Figs. 1 and 2); therefore, this supports a model that vimentin is more than an EMT biomarker and plays a functional role in lung adenocarcinoma invasion and metastasis. Despite decreased metastatic rates in the $KLV^{-/-}$ model, there is no survival advantage with vimentin depletion (Supplementary Fig. S2), which is consistent with previous reports demonstrating increased morbidity in vimentin-null mice (40). In the $KLV^{-/-}$ model, primary tumor burden could be exacerbating vimentin-dependent deficiencies in arterial remodeling (41) and wound healing (42).

EMT has been the canonical mechanism (9) for how cancer cells lose their epithelial morphology (4), invade through the basement membrane, and navigate the surrounding microenvironment (1, 43); however, this model is challenged in part by studies showing a more epithelial and collective-based migration by tumor cell clusters or packs (18, 44). The data presented here support the concept that a classical EMT does not occur in the majority of lung adenocarcinoma patients or in the lung adenocarcinoma *KLV* GEMM, but rather cancer cells undergo epithelial-like collective invasion and are surrounded by $vim^+/FSP1^+$ CAFs (Figs. 3 and 4). Across 96% of lung adenocarcinoma patient samples tested ($n = 26$), independent of driver mutation, vimentin was expressed in CAFs surrounding epithelial CIPs and only rarely in the tumor cells (Fig. 6). Similarly, vimentin was rarely expressed within the tumor cells of the $KLV^{+/+}$ GEMM, and only in the CAFs surrounding CIPs at the primary tumor site and at secondary metastatic lymph nodes (Figs. 3 and 4). This supports the concept that malignant cancer cells are not undergoing EMT but partnering with $vim^+/FSP1^+$ CAFs to potentially cometastasize to a secondary site (45). This finding is consistent with studies demonstrating that circulating tumor cell clusters have metastatic potential up to 50 times greater than single circulating tumor cells (46), suggesting that tumor cell cooperativity can lead to greater metastatic success. Furthermore, these heterotypic CAF-CIP clusters are enriched in early-stage lung adenocarcinoma patient samples (Fig. 6), indicating potential early dissemination (38, 47) of metastatic seeding.

Studies investigating vimentin within CAFs in homotypic (CAFs only) and heterotypic (CAFs + cancer cells) *in vitro* cell cultures demonstrate that vimentin drives not only homotypic CAF invasion, but also the formation and maintenance of heterotypic collective invasion chains (Fig. 5). We show that heterotypic invasive chains in vimentin-depleted CAFs are impaired compared with their wild-type counterparts. Nevertheless, some collective invasion remains suggesting compensatory or redundant mechanisms within vimentin-null CAFs. Because actin, focal adhesion kinase, and other components of the motility machinery (48) are not directly targeted, it is possible that some degree of vimentin-independent cell motility is maintained within the vimentin-depleted CAFs. This is also consistent with the *in vivo* studies showing that although significantly reduced, CIPs still form in the $KLV^{-/-}$ mice.

Taken together, the *in vivo* and *in vitro* data here support a model where vimentin is required for collective lung cancer invasion and metastasis by facilitating epithelial tumor cell CIP formation via CAF recruitment to the CIP. When vimentin function is impaired, heterotypic interactions are significantly reduced likely due to the inability of vimentin-depleted CAFs to move efficiently. These data support the claim that there are early-stage, epithelial, and

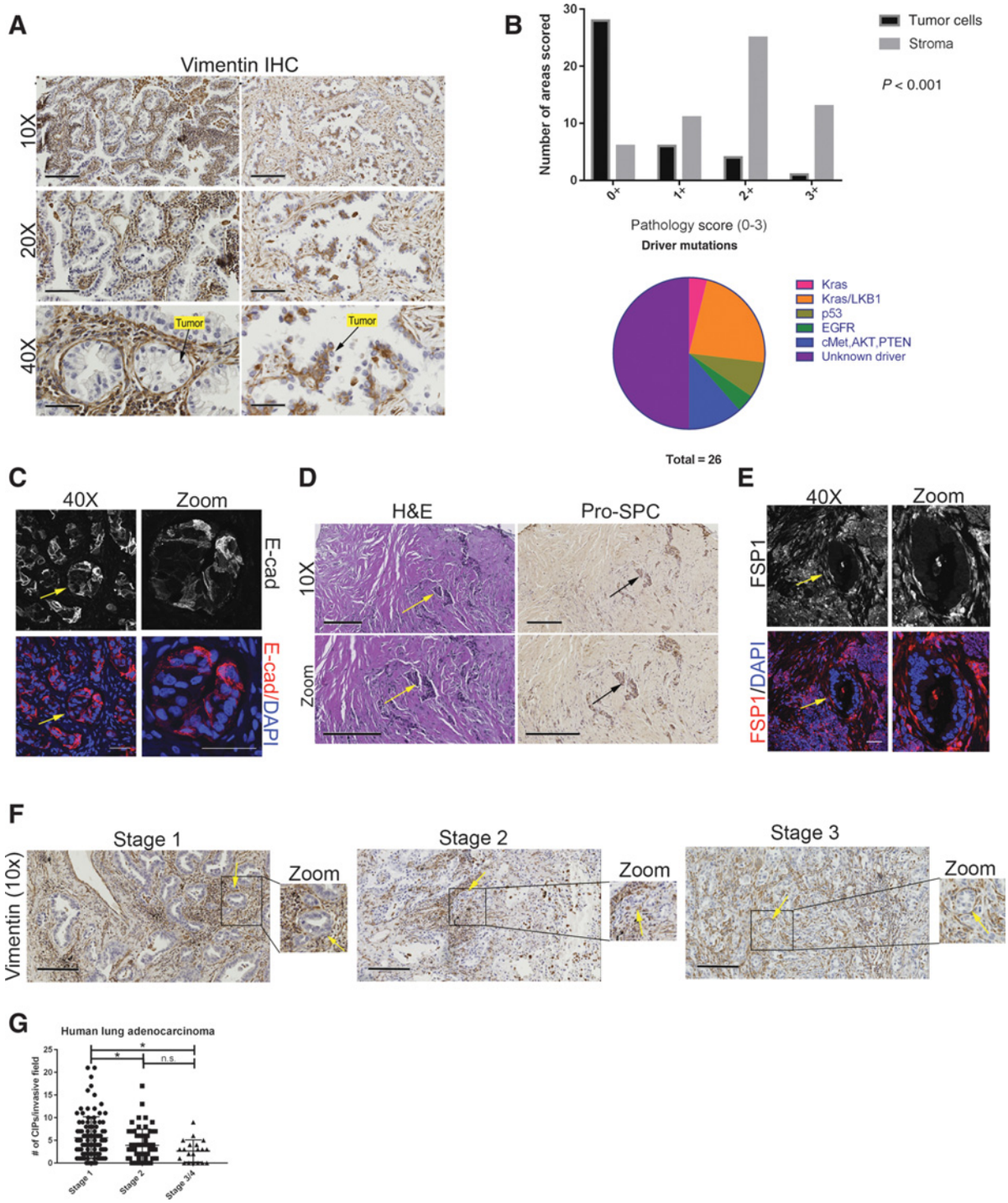


**Figure 6.**

Vimentin is expressed in CAFs of lung cancer patient CIPs, which lack EMT in tumor cells. **A,** Representative images of patient primary tumor samples stained for vimentin by immunohistochemistry (scale bars: 10x = 200 μm, 20x = 100 μm, 40x = 50 μm). **B,** Quantification of vimentin staining in tumor and stromal compartments. Pie chart of driver mutations in patient samples stained for vimentin. Statistical analysis was conducted using SAS Version 9.4. For the ordinal variable, frequency and average rank are calculated and presented. The univariate association of staining and different group, i.e., tumor cell and stroma were detect by the Wilcoxon Rank Sum test. **D,** Representative images of E-cadherin IF of human lung adenocarcinoma sample marking CIPs of tumor cells (40x = 50 μm). **D,** H&E and SPC staining of adenocarcinoma samples. CIPs marked with arrows (scale =200 μm). **E,** IF of FSP1 on Kras/LKB1 patient sample. CIP marked with an arrow (scale = 50 μm). **F,** Representative images of human lung adenocarcinoma samples stained for vimentin at stages 1–3. **G,** CIPs per invasive field by stage in human lung adenocarcinoma samples. Statistical significance determined by ANOVA with Tukey's multiple comparisons test ($P < 0.05$).

collective modes of lung cancer metastasis that drive cellular escape from the primary tumor and require vimentin-positive CAFs. We speculate that vimentin could be a target for antimetastatic therapies that are given at an early stage and in conjunction with traditional cytotoxics (49, 50).

## Disclosure of Potential Conflicts of Interest

No potential conflicts of interest were disclosed.

## Authors' Contributions

**Conception and design:** A.M. Richardson, L.S. Havel, A.E. Koyen, W.D. Martin, A.I. Marcus

**Development of methodology:** A.M. Richardson, L.S. Havel, A.E. Koyen, W.D. Martin, M. Gilbert-Ross, A.I. Marcus

**Acquisition of data (provided animals, acquired and managed patients, provided facilities, etc.):** A.M. Richardson, A.E. Koyen, J.M. Konen, J. Shupe, W.G. Wiles IV, W.D. Martin, G. Sica, M. Gilbert-Ross

**Analysis and interpretation of data (e.g., statistical analysis, biostatistics, computational analysis):** A.M. Richardson, A.E. Koyen, J.M. Konen, H.E. Grossniklaus, A.I. Marcus

**Writing, review, and/or revision of the manuscript:** A.M. Richardson, L.S. Havel, A.E. Koyen, J.M. Konen, J. Shupe, H.E. Grossniklaus, M. Gilbert-Ross, A.I. Marcus

**Administrative, technical, or material support (i.e., reporting or organizing data, constructing databases):** A.M. Richardson, J. Shupe, W.G. Wiles IV

**Study supervision:** A.M. Richardson, J. Shupe, A.I. Marcus

## Acknowledgments

This work was supported through funds from the NCI (1R01CA194027, 1RO1CA201340, and 1R01CA142858; awarded to A.I. Marcus and M. Gilbert-Ross) and through a Ruth L. Kirschstein National Research Service Award awarded (to A.M. Richardson). Grant 1U54 CA209992 was awarded to A.I. Marcus. The research in this publication was supported in part by the Winship Cancer Institute NCI/NIH funding (P30CA138292) and several Winship Core Facilities—the Emory Integrated Cellular Imaging, the Winship Core Pathology Laboratory, the Winship Biostatistics and Bioinformatics Shared Resource, and the Winship Cancer Animal Models Core. Special thanks to Jamie Arnst, Rachel Commander, Jamie King, Junghui Koo, Janna Mouw, Brian Pedro, Katelyn Ponder, Emily Summerbell, Carol Tucker-Burden, and Paula Vertino for helpful discussions and technical advice.

The costs of publication of this article were defrayed in part by the payment of page charges. This article must therefore be hereby marked *advertisement* in accordance with 18 U.S.C. Section 1734 solely to indicate this fact.

Received June 21, 2017; revised October 10, 2017; accepted October 30, 2017; published OnlineFirst December 5, 2017.

## References

1. Tse JC, Kalluri R. Mechanisms of metastasis: epithelial-to-mesenchymal transition and contribution of tumor microenvironment. J Cell Biochem 2007;101:816–29.
2. Lamouille S, Xu J, Derynck R. Molecular mechanisms of epithelial-mesenchymal transition. Nat Rev Mol Cell Biol 2014;15:178–96.
3. Serrano-Gomez SJ, Maziveyi M, Alahari SK. Regulation of epithelial-mesenchymal transition through epigenetic and post-translational modifications. Mol Cancer 2016;15:18.
4. Onder TT, Gupta PB, Mani SA, Yang J, Lander ES, Weinberg RA. Loss of E-cadherin promotes metastasis via multiple downstream transcriptional pathways. Cancer Res 2008;68:3645–54.
5. Huber MA, Kraut N, Beug H. Molecular requirements for epithelial-mesenchymal transition during tumor progression. Curr Opin Cell Biol 2005;17:548–58.
6. Chaffer CL, San Juan BP, Lim E, Weinberg RA. EMT, cell plasticity and metastasis. Cancer Metastasis Rev 2016;35:645–54.
7. Zeisberg M, Neilson EG. Biomarkers for epithelial-mesenchymal transitions. J Clin Invest 2009;119:1429–37.
8. Yao D, Dai C, Peng S. Mechanism of the mesenchymal-epithelial transition and its relationship with metastatic tumor formation. Mol Cancer Res 2011;9:1608–20.
9. Thiery JP. Epithelial-mesenchymal transitions in tumour progression. Nat Rev Cancer 2002;2:442–54.
10. Fischer KR, Durrans A, Lee S, Sheng J, Li F, Wong ST, et al. Epithelial-to-mesenchymal transition is not required for lung metastasis but contributes to chemoresistance. Nature 2015;527:472–6.
11. Zheng X, Carstens JL, Kim J, Scheible M, Kaye J, Sugimoto H, et al. Epithelial-to-mesenchymal transition is dispensable for metastasis but induces chemoresistance in pancreatic cancer. Nature 2015;527:525–30.
12. Siegel RL, Miller KD, Jemal A. Cancer statistics, 2016. CA Cancer J Clin 2016;66:7–30.
13. Sanchez-Cespedes M. The role of LKB1 in lung cancer. Fam Cancer 2011;10:447–53.
14. Chen Z, Cheng K, Walton Z, Wang Y, Ebi H, Shimamura T, et al. A murine lung cancer co-clinical trial identifies genetic modifiers of therapeutic response. Nature 2012;483:613–7.
15. Ji H, Ramsey MR, Hayes DN, Fan C, McNamara K, Kozlowski P, et al. LKB1 modulates lung cancer differentiation and metastasis. Nature 2007;448:807–10.
16. Kottakis F, Nicolay BN, Roumane A, Karnik R, Gu H, Nagle JM, et al. LKB1 loss links serine metabolism to DNA methylation and tumorigenesis. Nature 2016;539:390–5.
17. Shackelford DB, Abt E, Gerken L, Vasquez DS, Seki A, Leblanc M, et al. LKB1 inactivation dictates therapeutic response of non-small cell lung cancer to the metabolism drug phenformin. Cancer Cell 2013;23:143–58.
18. Gilbert-Ross M, Konen J, Koo J, Shupe J, Robinson BS, Wiles WGt, et al. Targeting adhesion signaling in KRAS, LKB1 mutant lung adenocarcinoma. JCI Insight 2017;2:e90487.
19. Gao Y, Xiao Q, Ma H, Li L, Liu J, Feng Y, et al. LKB1 inhibits lung cancer progression through lysyl oxidase and extracellular matrix remodeling. Proc Natl Acad Sci U S A 2010;107:18892–7.
20. Colucci-Guyon E, Portier MM, Dunia I, Paulin D, Pournin S, Babinet C. Mice lacking vimentin develop and reproduce without an obvious phenotype. Cell 1994;79:679–94.
21. Liu S, Liu L, Ye W, Ye D, Wang T, Guo W, et al. High vimentin expression associated with lymph node metastasis and predicated a poor prognosis in oral squamous cell carcinoma. Sci Rep 2016;6:38834.
22. Thomas PA, Kirschmann DA, Cerhan JR, Folberg R, Seftor EA, Sellers TA, et al. Association between keratin and vimentin expression, malignant phenotype, and survival in postmenopausal breast cancer patients. Clin Cancer Res 1999;5:2698–703.
23. Javle MM, Gibbs JF, Iwata KK, Pak Y, Rutledge P, Yu J, et al. Epithelial-mesenchymal transition (EMT) and activated extracellular signal-regulated kinase (p-Erk) in surgically resected pancreatic cancer. Ann Surg Oncol 2007;14:3527–33.
24. Dauphin M, Barbe C, Lemaire S, Nawrocki-Raby B, Lagonotte E, Delepine G, et al. Vimentin expression predicts the occurrence of metastases in non small cell lung carcinomas. Lung Cancer 2013;81:117–22.
25. Burch TC, Watson MT, Nyalwidhe JO. Variable metastatic potentials correlate with differential plectin and vimentin expression in syngeneic androgen independent prostate cancer cells. PLoS One 2013;8:e65005.
26. Domagala W, Lasota J, Dukowicz A, Markiewski M, Striker G, Weber K, et al. Vimentin expression appears to be associated with poor prognosis in node-negative ductal NOS breast carcinomas. Am J Pathology 1990;137:1299–304.
27. Chung BM, Rotty JD, Coulombe PA. Networking galore: intermediate filaments and cell migration. Curr Opin Cell Biol 2013;25:600–12.
28. Helfand BT, Mendez MG, Murthy SN, Shumaker DK, Grin B, Mahammad S, et al. Vimentin organization modulates the formation of lamellipodia. Mol Biol Cell 2011;22:1274–89.
29. Ivaska J, Pallari HM, Nevo J, Eriksson JE. Novel functions of vimentin in cell adhesion, migration, and signaling. Exp Cell Res 2007;313:2050–62.

30. Havel LS, Kline ER, Salgueiro AM, Marcus AI. Vimentin regulates lung cancer cell adhesion through a VAV2-Rac1 pathway to control focal adhesion kinase activity. Oncogene 2015;34:1979–90.
31. Mendez MG, Kojima S, Goldman RD. Vimentin induces changes in cell shape, motility, and adhesion during the epithelial to mesenchymal transition. FASEB J 2010;24:1838–51.
32. Zhu QS, Rosenblatt K, Huang KL, Lahat G, Brobey R, Bolshakov S, et al. Vimentin is a novel AKT1 target mediating motility and invasion. Oncogene 2011;30:457–70.
33. Konen J, Wilkinson S, Lee B, Fu H, Zhou W, Jiang Y, et al. LKB1 kinase-dependent and -independent defects disrupt polarity and adhesion signaling to drive collagen remodeling during invasion. Mol Biol Cell 2016;27:1069–84.
34. DuPage M, Dooley AL, Jacks T. Conditional mouse lung cancer models using adenoviral or lentiviral delivery of Cre recombinase. Nat Protoc 2009;4:1064–72.
35. Mao P, Wu S, Li J, Fu W, He W, Liu X, et al. Human alveolar epithelial type II cells in primary culture. Physiol Rep 2015;3.
36. Augsten M. Cancer-associated fibroblasts as another polarized cell type of the tumor microenvironment. Front Oncol 2014;4:62.
37. Konen J, Summerbell E, Dwivedi B, Galior K, Hou Y, Rusnak L, et al. Image-guided genomics of phenotypically heterogeneous populations reveals vascular signaling during symbiotic collective cancer invasion. Nat Commun 2017;8:15078.
38. Hosseini H, Obradovic MM, Hoffmann M, Harper KL, Sosa MS, Werner-Klein M, et al. Early dissemination seeds metastasis in breast cancer. Nature 2016 Dec 14. [Epub ahead of print].
39. Tian W, Wang G, Yang J, Pan Y, Ma Y. Prognostic role of E-cadherin and Vimentin expression in various subtypes of soft tissue leiomyosarcomas. Med Oncol 2013;30:401.
40. Terzi F, Henrion D, Colucci-Guyon E, Federici P, Babinet C, Levy BI, et al. Reduction of renal mass is lethal in mice lacking vimentin. Role of endothelin-nitric oxide imbalance. J Clin Invest 1997;100:1520–8.
41. Schiffers PM, Henrion D, Boulanger CM, Colucci-Guyon E, Langa-Vuves F, van Essen H, et al. Altered flow-induced arterial remodeling in vimentin-deficient mice. Arterioscler Thromb Vasc Biol 2000;20:611–6.
42. Eckes B, Colucci-Guyon E, Smola H, Nodder S, Babinet C, Krieg T, et al. Impaired wound healing in embryonic and adult mice lacking vimentin. J Cell Sci 2000;113(Pt 13):2455–62.
43. van Zijl F, Krupitza G, Mikulits W. Initial steps of metastasis: cell invasion and endothelial transmigration. Mutat Res 2011;728:23–34.
44. Cheung KJ, Gabrielson E, Werb Z, Ewald AJ. Collective invasion in breast cancer requires a conserved basal epithelial program. Cell 2013;155:1639–51.
45. Duda DG, Duyverman AM, Kohno M, Snuderl M, Steller EJ, Fukumura D, et al. Malignant cells facilitate lung metastasis by bringing their own soil. Proc Natl Acad Sci U S A 2010;107:21677–82.
46. Aceto N, Bardia A, Miyamoto DT, Donaldson MC, Wittner BS, Spencer JA, et al. Circulating tumor cell clusters are oligoclonal precursors of breast cancer metastasis. Cell 2014;158:1110–22.
47. Roychowdhury A, Samadder S, Islam MS, Chaudhury K, Roy A, Banerjee D, et al. Identification of changes in the human papilloma virus 16 (HPV16) genome during early dissemination of cervical cancer cells may complement histological diagnosis of lymph node metastasis. Pathol Oncol Res 2017;23:845–52.
48. McLean GW, Carragher NO, Avizienyte E, Evans J, Brunton VG, Frame MC. The role of focal-adhesion kinase in cancer - a new therapeutic opportunity. Nat Rev Cancer 2005;5:505–15.
49. Yang Z, Garcia A, Xu S, Powell DR, Vertino PM, Singh S, et al. Withania somnifera root extract inhibits mammary cancer metastasis and epithelial to mesenchymal transition. PLoS One 2013;8:e75069.
50. Lee J, Hahm ER, Marcus AI, Singh SV. Withaferin A inhibits experimental epithelial-mesenchymal transition in MCF-10A cells and suppresses vimentin protein level in vivo in breast tumors. Mol Carcinog 2015;54:417–29.